© 2020 Chinese Physical Society and IOP Publishing Ltd Printed in China and the UK

Commun. Theor. Phys. **72** (2020) 085201 (8pp) https://doi.org/10.1088/1572-9494/ab8a19

Single top partner production in the *tZ* channel at $e\gamma$ collision in the littlest Higgs model with T-parity

Bingfang Yang (杨炳方)[1], **Hengheng Bi** (毕恒恒)[1], **Biaofeng Hou** (侯镖锋)[2] and **Bingjie Wu** (武冰洁)[3,4]

[1] School of Physics, Henan Normal University, Xinxiang 453007, China
[2] College of Physical Science and Technology, Central China Normal University, Wuhan 430079, China
[3] College of Physics and Electronic Engineering, Zhengzhou Normal University, Zhengzhou 450044, China

E-mail: wubj0506@126.com

Received 19 January 2020, revised 1 April 2020
Accepted for publication 3 April 2020
Published 20 July 2020

Abstract

Introducing the top partner is a common way to cancel the largest quadratically divergent contribution to the Higgs mass induced by the top quark. In this work, we study single top partner production in the *tZ* channel at $e\gamma$ collision in the littlest Higgs model with T-parity (LHT). Since it is well known that polarized beams can enhance the cross section, we analyze the signal via polarized electron beams, and photon beams. we have selected two decay modes for comparison, based on the leptonic or the hadronic decays of the *W* and *Z* from the top partner. We then construct a detailed detector simulation, and choose a set of cuts to enhance signal significance. For mode A(B), the capacity for exclusion in this process at $\sqrt{s} = 3$ TeV is comparable to the current experimental limits with $L = 1000$ (500) fb^{-1}. If the integrated luminosity can be increased to 3000 fb^{-1}, the top partner mass m_{T_+} can be excluded up to 1350 (1440) GeV at 2σ level. We also considered the initial state radiation effect, and find that this effect reduces the excluding ability of the $e\gamma$ collision on the the top partner mass by approximately 10 GeV. Moreover, the ability to exclude the LHT parameter space at $e\gamma$ collision complements the existing research.

Keywords: littlest Higgs model with T-parity, top partner, new physics, eγ collider

(Some figures may appear in colour only in the online journal)

1. Introduction

In 2012, the Higgs boson, with a mass ∼125 GeV, was discovered by experiments at the Large Hadron Collider (LHC) [1, 2], which opens a window for us to understand electroweak symmetry breaking. However, the Higgs mass in the standard model (SM) is quadratically divergent, which leads to fine-tuning problems [3]. In order to solve this problem, many new physics models beyond the SM have been proposed, such as extra dimensions [4], composite Higgs [5], little Higgs [6], twin Higgs [7], supersymmetric models [8], etc. In these models, vector-like quarks (VLQs) are introduced in order to alleviate the fine-tuning problem. VLQs are hypothetical spin-1/2 colored particles with left-handed and right-handed components that transform in the same way as the SM gauge group. The vector-like top partners in the VLQs have attracted a great deal of attention, since they cancel the largest quadratic divergence induced by the top quark loop. Many relevant studies of the vector-like top partner have been conducted in recent years [9].

The search for vector-like top partner *T* at LHC-13 TeV has been analyzed by ATLAS and CMS collaborations [10, 11]. This excludes top partner masses in the range 900 ∼ 1300 GeV at a 95% confidence level, and with an integrated luminosity of about 36 fb^{-1}. Compared to the LHC, however, lepton colliders have a cleaner background, enabling the precise investigation of the properties of various particles. In recent years, many lepton collider schemes have been put forward, such as the Circular Electron Positron Collider (CEPC) [12], the International Linear

[4] Author to whom any correspondence should be addressed.

Collider (ILC)[13], and the Compact Linear Collider (CLIC) [14]; these can run at variable center-of-mass energy ($\sqrt{s}$) ranging from 500 GeV to 3 TeV. In addition to e^+e^- collision, these colliders can also realize $\gamma\gamma$ and $e\gamma$ collisions by means of the backward Compton scattering of incident electron- and laser beams. For the e^+e^- and $\gamma\gamma$ collision modes, the top partner needs to be pair produced ($e^+e^-/\gamma\gamma \to T\bar{T}$), or single produced with four-body final state ($e^+e^-/\gamma\gamma \to e^-\nu_e T\bar{b}$), so that their cross sections are much smaller than that at the $e\gamma$ collision. The $e\gamma$ collision exhibits unique properties to enable further investigations in the field of of single top partner physics, particularly in the case of polarized beams. It has the capacity to perform precise cross section measurements, due to large counting rates, and the absence of $t\bar{t}$ pair production background. In this work, we will study the search for single vector-like top partner production through the tZ channel at $e\gamma$ collision in the littlest Higgs model with T-parity (LHT) model [15].

The remainder of this paper is organized as follows: Firstly, we briefly introduce the top partner in the LHT model in section 2. Next, we generate the the signal and background events, and study the discovery potentiality of the T-even top partner T_+ decaying to tZ at the high energy $e\gamma$ collision in section 3, where two decay final states are considered. Finally, we give our conclusions in section 4.

2. Top partner in the LHT model

The LHT model is a non-linear sigma model, based on a $SU(5)$ global symmetry, broken down to $SO(5)$ at scale $f \sim \mathcal{O}$(TeV) by the vacuum expectation value (VEV) of the Σ field:

$$\Sigma_0 = \begin{pmatrix} & & \mathbf{1}_{2\times 2} \\ & 1 & \\ \mathbf{1}_{2\times 2} & & \end{pmatrix}. \tag{1}$$

The breaking of global symmetry gives rise to 14 Goldstone bosons. Simultaneously, the gauge group $[SU(2) \times U(1)]_1 \times [SU(2) \times U(1)]_2$ is also broken down to the diagonal SM electroweak group $SU(2)_L \times U(1)_Y$. Following the breaking of electroweak symmetry, 4 new gauge bosons $W_H^{\pm}$, Z_H, A_H eat 4 Goldstone bosons and acquire mass, given at $\mathcal{O}(v^2/f^2)$ by

$$\begin{aligned} M_{W_H} &= M_{Z_H} = gf\left(1 - \frac{v^2}{8f^2}\right), \\ M_{A_H} &= \frac{g'f}{\sqrt{5}}\left(1 - \frac{5v^2}{8f^2}\right), \end{aligned} \tag{2}$$

where g and g' are respectively the SM $SU(2)_L$ and $U(1)_Y$ gauge couplings, and the VEV v must be redefined as:

$$\begin{aligned} v &= \frac{f}{\sqrt{2}}\arccos\left(1 - \frac{v_{\rm SM}^2}{f^2}\right) \\ &\simeq v_{\rm SM}\left(1 + \frac{1}{12}\frac{v_{\rm SM}^2}{f^2}\right), \end{aligned} \tag{3}$$

with $v_{\rm SM} = 246$ GeV.

In the top sector of this model, an additional vector-like top partner T_+ is introduced to cancel the quadratically divergent contribution to Higgs mass caused by the top quark loop. The top partner T_+ is T-even, the implementation of T-parity also requires its T-odd mirror partner T_-. Following symmetry breaking, the top quark and its partners acquire mass, given at $\mathcal{O}(v^2/f^2)$, by:

$$\begin{aligned} m_t &= \frac{\lambda_2 vR}{\sqrt{1+R^2}}\left[1 + \frac{v^2}{f^2}\left(-\frac{1}{3} + \frac{1}{2}\frac{R^2}{(1+R^2)^2}\right)\right] \\ m_{T_+} &= \frac{f}{v}\frac{m_t(1+R^2)}{R}\left[1 + \frac{v^2}{f^2}\left(\frac{1}{3} - \frac{R^2}{(1+R^2)^2}\right)\right] \\ m_{T_-} &= \frac{f}{v}\frac{m_t\sqrt{1+R^2}}{R}\left[1 + \frac{v^2}{f^2}\left(\frac{1}{3} - \frac{1}{2}\frac{R^2}{(1+R^2)^2}\right)\right], \end{aligned} \tag{4}$$

where $R = \lambda_1/\lambda_2$ is a dimensionless ratio, and λ_1 and λ_2 are two top quark Yukawa couplings. Since the T_+ mass is always larger than the T-odd top partner T_- mass, T_+ can then decay into $A_H T_-$, apart from the usual decay modes (Wb, tZ, th).

3. Event generation and discovery potentiality

In figure 1, we show the leading order Feynman diagrams of single $\bar{T}_+$ production at $e^-\gamma$ collision in the LHT model. We can see that these Feynman diagrams are the same as those of the SM, except that the SM top quark is replaced here by the heavy top partner. The new coupling vertexes, $\bar{T}_+Wb$ and $\bar{T}_+Zt$, involved in our calculation are given by:

$$\bar{T}_+W^{+\mu}b: \quad \frac{ig}{\sqrt{2}}(V_{\rm CKM})_{tb}\frac{R^2}{1+R^2}\frac{v}{f}[1 + \frac{v^2}{f^2}d_2]\gamma^\mu P_L \tag{5}$$

$$\bar{T}_+Z^\mu t: \quad \frac{ig}{\cos\theta_W}\frac{R}{2}\frac{v}{f}\left[1 + \frac{v^2}{f^2}\left(d_2 - \frac{R^2}{2}\right)\right]\gamma^\mu P_L \tag{6}$$

$$\text{with:} \quad d_2 = -\frac{5}{6} + \frac{1}{2}\left(\frac{R}{1+R^2}\right)^2(R^2+4), \tag{7}$$

where $P_L = \dfrac{1-\gamma_5}{2}$ is the chiral projection operator and $(V_{\rm CKM})_{tb}$ is one CKM element.

In the $e\gamma$ collision mode, the use of polarized e^- beams and photon beams is advantageous. Therefore, we show the ratio σ_P/σ of $e^-\gamma \to \bar{T}_+b\nu_e$ cross sections at two different polarizations, P_{e^-} and P_γ , in figure 2, where $f = 800$ GeV, $R = 1$ (corresponding to $m_T \approx 1120$ GeV), and $\sqrt{s} = 2$ TeV are selected as examples. We can see that the cross section has the largest value at $P_e = -1$, and $P_\gamma = 1$, which can be explained as follows:

In the case of extreme relativity, the electron, neutrino, and b quark tend to be left-handed and their anti-particles tend to be right-handed. Due to weak $V-A$ interaction, only the left-handed electron exhibits coupling with the W boson, so that the polarized cross sections decrease as the value $P_e \to 1$, and vanish when $P_e = 1$. Due to the conservation of angular momentum, the initial photon in vertex $\gamma e^- e^+$ of figure 1(b) tends to be left-handed, based on the initial left-handed

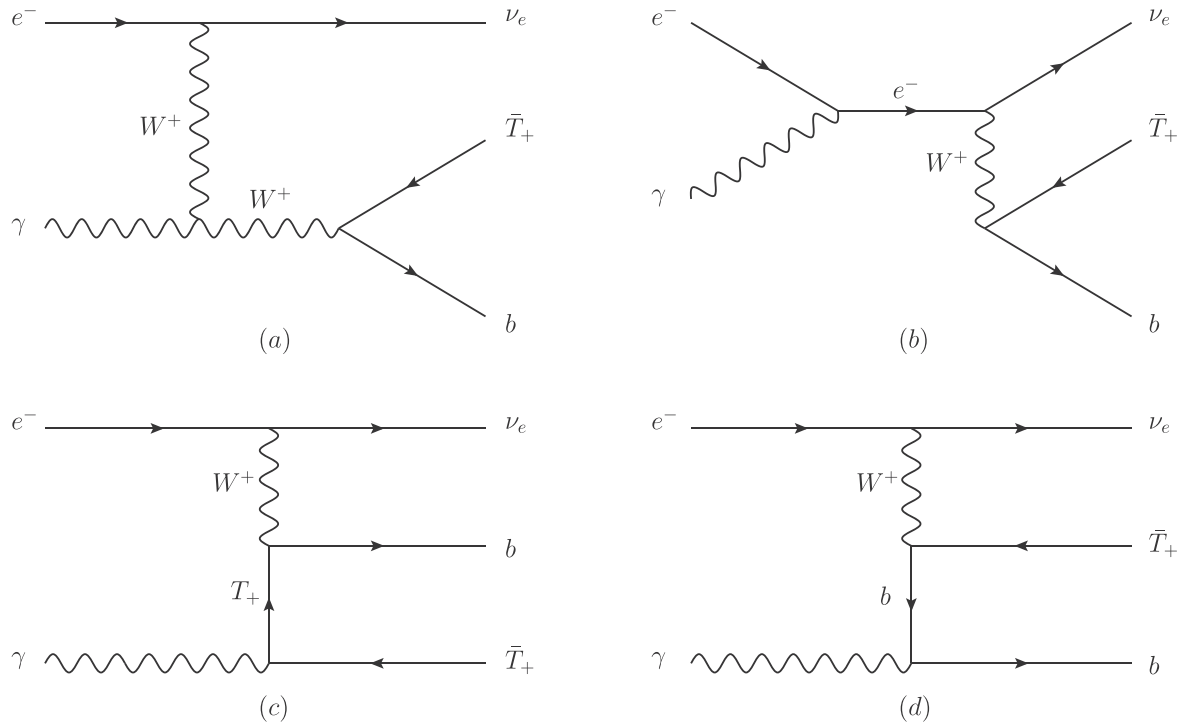

Figure 1. The leading order Feynman diagrams of single $\bar{T}_+$ production at $e^-\gamma$ collision.

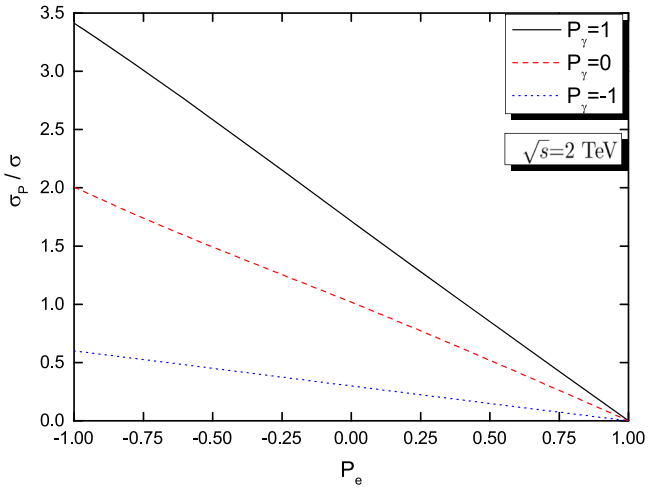

Figure 2. The ratio σ_P/σ of $e^-\gamma \to \bar{T}_+ b\nu_e$ cross sections at polarizations P_{e^-} and P_γ, for $f = 800$ GeV, $R = 1$ ($m_T \approx 1120$ GeV) at $\sqrt{s} = 2$ TeV. σ_P denotes the polarized cross section, and σ denotes the unpolarized cross section.

electron, and the photon in vertex $\gamma b\bar{b}$ of figure 1 (d) tends to be right-handed, based on the final left-handed b quark. The initial photons in figure 1 (a) and figure 1 (c) can be left-handed or right-handed. Moreover, the largest contribution comes from the figure 1(d), so that the total cross section is dominated by the right-hand photon.

We can see that the proper polarized beam effectively enhances the cross section. Due to the technical limit of maximum polarization, we can only reach a value close to $P_{e^-} \times P_\gamma = -0.8$ for the incident beam. Therefore, we have selected $P_{e^-} = -0.8$ and $P_\gamma = +1$ for the following calculations.

In this work, we consider single vector-like top partner production in the tZ channel at $e\gamma$ collision. For comparison, we have selected two decay modes for the final state signals, dependent on the leptonic or the hadronic decays of the W^- and Z from the top partner, thus:

Mode A: $e^-\gamma \to \bar{T}_+ b\nu_e \to (\bar{t}Z)b\nu_e \to (W^-\bar{b}l^+l^-)b\nu_e \to (jj\bar{b}l^+l^-)b\nu_e$.
Mode B: $e^-\gamma \to \bar{T}_+ b\nu_e \to (\bar{t}Z)b\nu_e \to (W^-\bar{b}jj)b\nu_e \to (l^-\bar{\nu}_l\bar{b}jj)b\nu_e$.

Following analysis, the main backgrounds originate from the processes $e^-\gamma \to W^-ZZ\nu_e$, $e^-\gamma \to t\bar{t}W^-\nu_e$, $e^-\gamma \to ZW^-h\nu_e$, and $e^-\gamma \to \bar{t}bZ\nu_e$. For clarity, we summarize these signal and background processes in table 1.

In the following calculations, there are only two relevant LHT model parameters, i.e. the scale f and the ratio R. The relevant SM input parameters [16] are taken as follows:

$$m_t = 173.0\ \text{GeV}, m_Z = 91.1876\ \text{GeV}, \quad m_h = 125\ \text{GeV},$$
$$\sin^2\theta_W = 0.231, \quad \alpha(m_Z) = 1/128.$$

We generate signal and background events with MG5_aMC_v2.3.3 [17], then transmit these parton-level events to **Pythia 6** [18] for showering and hadronization. We construct fast detector simulations using **Delphes** [19], and cluster jets by **Fastjet** [20] with the $anti-k_t$ algorithm [21], where the distance parameter $\Delta R = 0.4$. Finally, we analyze the reconstructed-level events using **MadAnalysis 5** [22]. We use EasyScan_HEP [23] to connect these programs, and to scan the parameter space.

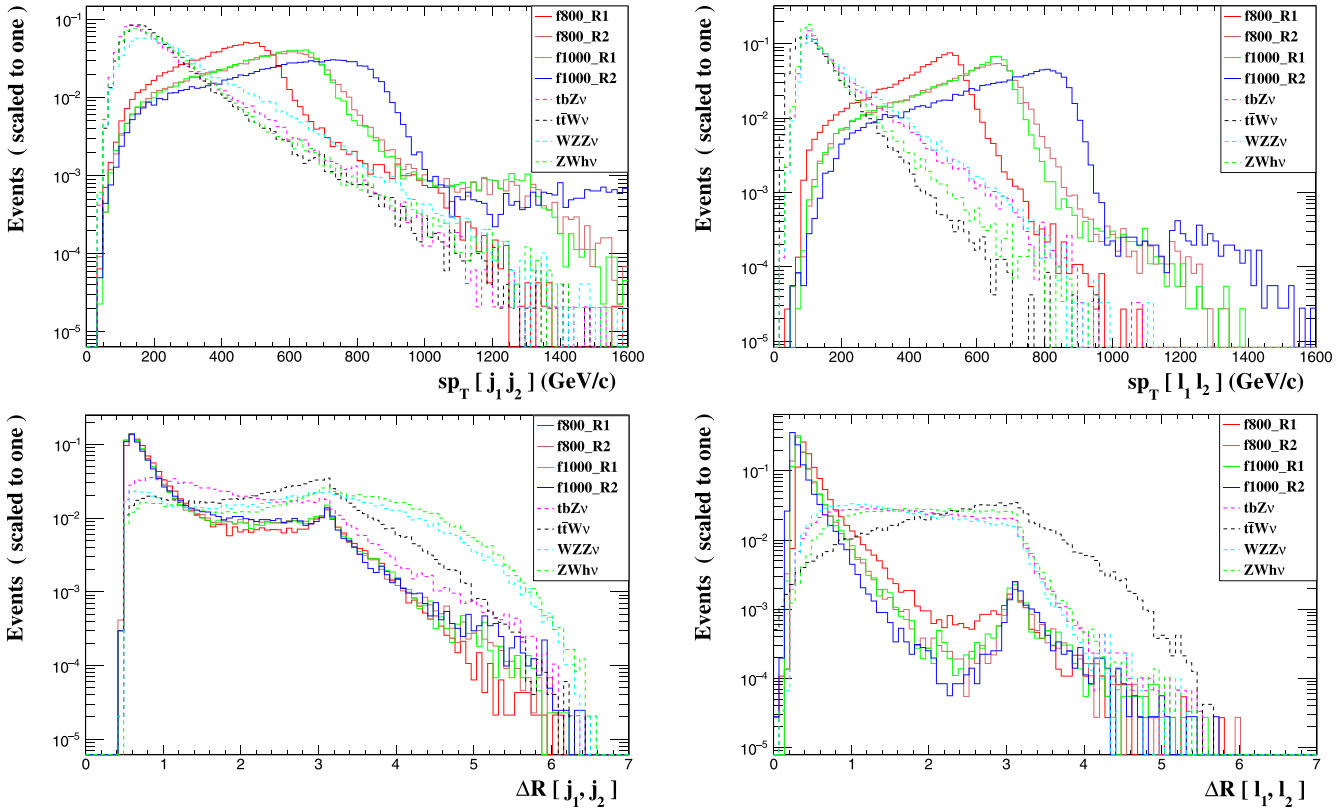

Figure 3. Normalized distributions of $sp_T(j_1, j_2)$, $sp_T(l_1, l_2)$, $\Delta R(j_1, j_2)$, $\Delta R(l_1, l_2)$ in the polarized signals and backgrounds for the four signal benchmark points at $\sqrt{s} = 2$ TeV in mode A.

Table 1. The processes of signals (S) and backgrounds (B) for two modes.

	Process	Mode A	Mode B
S	$e^-\gamma \to \bar{T}_+ b\nu_e$	$\bar{T}_+ \to \bar{t}Z, \bar{t} \to jj\bar{b}, Z \to l^+l^-$	$\bar{T}_+ \to \bar{t}Z, \bar{t} \to l^-\bar{\nu}_l\bar{b}, Z \to jj$
B_1	$e^-\gamma \to W^-ZZ\nu_e$	$W^- \to jj, Z_1 \to l^+l^-, Z_2 \to b\bar{b}$	$W^- \to l^-\bar{\nu}_l, Z_1 \to jj, Z_2 \to b\bar{b}$
B_2	$e^-\gamma \to t\bar{t}W^-\nu_e$	$t \to l^+\nu_l b, \bar{t} \to W^-\bar{b}\ W_1^- \to l^-\bar{\nu}_l, W_2^- \to jj$	$t \to jjb, \bar{t} \to W^-\bar{b}\ W_1^- \to l^-\bar{\nu}_l, W_2^- \to jj$
B_3	$e^-\gamma \to ZW^-h\nu_e$	$Z \to l^+l^-, W^- \to jj, h \to b\bar{b}$	$Z \to jj, W^- \to l^-\bar{\nu}_l, h \to b\bar{b}$
B_4	$e^-\gamma \to \bar{t}bZ\nu_e$	$\bar{t} \to jj\bar{b}, Z \to l^+l^-$	$\bar{t} \to l^-\bar{\nu}_l\bar{b}, Z \to jj$

In this paper, we have selected four signal benchmark points as examples:

- f800_R1: $f = 800$ GeV, $R = 1$ ($m_T \approx 1120$ GeV);
- f800_R2: $f = 800$ GeV, $R = 2$ ($m_T \approx 1440$ GeV);
- f1000_R1: $f = 1000$ GeV, $R = 1$ ($m_T \approx 1440$ GeV);
- f1000_R2: $f = 1000$ GeV, $R = 2$ ($m_T \approx 1750$ GeV).

3.1. Mode A, $W^- \to jj$ and $Z \to l^+l^-$

In this section, we will study the exclusion ability of $e\gamma$ collision relating to top partner mass in mode A. In order to improve the signal-to-background ratio, some cuts of kinematic distributions for the final states are required. Since the Z boson in the signal originates from top partner decay, whereas other Z bosons in the backgrounds originate from direct production during the processes, this will provide the main difference between the signal and the backgrounds. Therefore we will focus on this feature when selecting the cuts. Although the b-jets exhibit high tagging efficiency, we find that there is no good distinction between the b-jet distributions of signals and backgrounds. In addition, we find the kinematic distributions of the signals and backgrounds for the center-of-mass energy $\sqrt{s} = 2$ TeV are similar to those for $\sqrt{s} = 3$ TeV. In figure 3, we show the related normalized distributions of $sp_T(j_1, j_2)$, $sp_T(l_1, l_2)$, $\Delta R(j_1, j_2)$, and $\Delta R(l_1, l_2)$ in the polarized signals and backgrounds for the four signal benchmark points at $\sqrt{s} = 2$ TeV, where $sp_T = |p_T^1| + |p_T^2|$ is the sum of the transverse momentum of the related particles, $\Delta R(x, y) = \sqrt{(\Delta\phi)^2 + (\Delta\eta)^2}$ with $\Delta\phi$ is the difference of azimuthal angle between object x and y, and $\Delta\eta$ gives the difference of pseudo-rapidity between them, $x, y = l, j$. We note that the final state jets and leptons in the signal events demonstrate greater transverse momentum and closer distance than in the backgrounds, due to the large mass

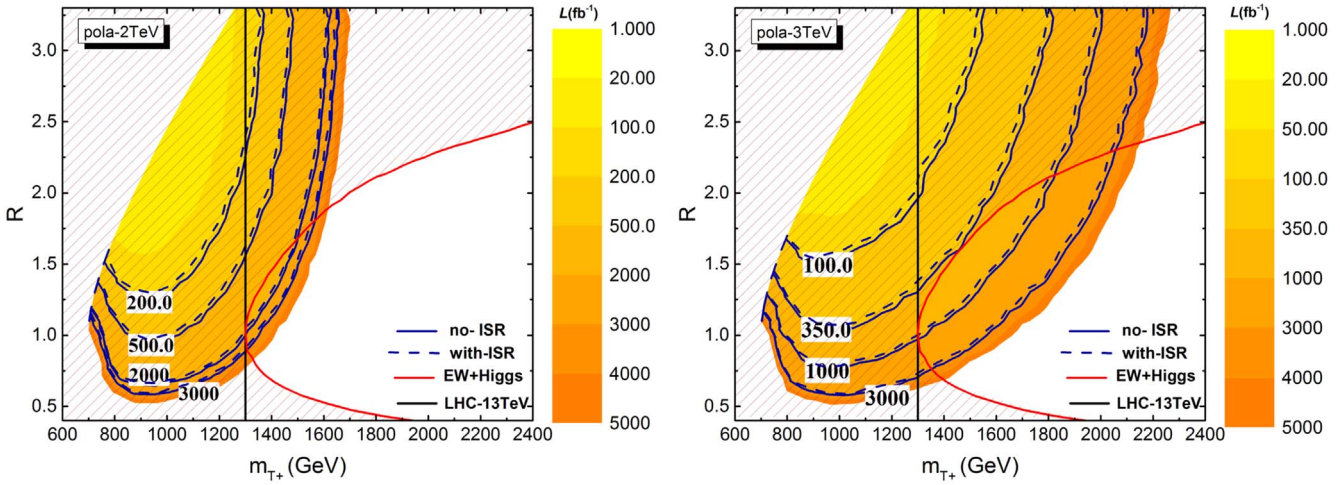

Figure 4. 2σ exclusion limit in $R - m_{T_+}$ plane at $\sqrt{s} = 2$ TeV (left) and $\sqrt{s} = 3$ TeV (right). Contour plot of excluding capability at different integrated luminosities, where ISR effects are indicated by dashed blue lines, and solid blue lines indicate where ISR effects are not included. The black numbers in white box denote different integrated luminosities. The red solid line denotes the 2σ limit from the global fit of EWPO and Higgs data, and the black solid lines denote the limit based on the LHC-13 TeV.

Table 2. Cut flows of the signals and backgrounds at $\sqrt{s} = 2$ TeV and $\sqrt{s} = 3$ TeV (in parentheses) with polarized beam for the four signal benchmark points in mode A.

	Signals ($\times 10^{-3}$fb)				Backgrounds ($\times 10^{-3}$fb)			
Benchmarks	f800_R1	f800_R2	f1000_R1	f1000_R2	$tbZ\nu$	$t\bar{t}W\nu$	$WZZ\nu$	$ZWh\nu$
Original	21(35)	24(71)	7.9(20)	3.3(32)	192(302)	439(806)	559(1099)	232(464)
Trigger	14(24)	15(44)	5.1(13)	1.9(18)	109(161)	204(293)	329(604)	130(235)
cut1	11(19)	13(39)	4.4(11)	1.7(16)	24(51)	35(68)	106(254)	28(69)
cut2	11(18)	13(38)	4.3(11)	1.7(16)	7.7(19)	2.8(8.2)	26(80)	5.6(17)
cut3	7.9(12)	8.7(23)	2.9(6.9)	1.1(9.1)	4.1(8.9)	0.8(2.4)	4.9(12)	1.8(4.7)
cut4	7.0(11)	8.2(22)	2.7(6.5)	1.0(8.7)	2.5(5.6)	0.009(0.06)	2.9(8.2)	0.9(2.8)
Total Eff.	33% (32%)	34% (31%)	34% (32%)	31% (27%)	1.3% (1.9%)	0.002% (0.008%)	0.5% (0.75%)	0.4% (0.6%)

of the top partner. Based on the behavioral characteristics of these distributions, we impose the following cuts, in order to enhance the signal significance:

$$\begin{aligned}
&\text{Trigger:}\ \ N(j) \geqslant 2, N(l) \geqslant 2;\\
&\text{Cut}-1:\ \ sp_T(j_1, j_2) > 300\ \text{GeV};\\
&\text{Cut}-2:\ \ sp_T(l_1, l_2) > 300\ \text{GeV};\\
&\text{Cut}-3:\ \ \Delta R(j_1, j_2) < 1.0;\\
&\text{Cut}-4:\ \ \Delta R(l_1, l_2) < 0.6.
\end{aligned}$$

For clarity, we summarize the cut flows of the signals and backgrounds for the four signal benchmark points in table 2. We note that the dominant background is process $WZZ\nu$, which is followed by process $t\bar{t}W\nu$. These cuts suppress the backgrounds and isolate the signal effectively. For the four benchmarks, the total cut efficiencies of the signals achieve 33% (32%), 34% (31%), 34% (32%), and 31% (27%) for the $\sqrt{s} = 2$ TeV ($\sqrt{s} = 3$ TeV), respectively. Conservatively, we take the same cuts for all the signal parameter points at $\sqrt{s} = 2$, 3 TeV in the following calculations.

Initial state radiation (ISR) significantly affects cross sections [24], particularly in the case of lepton colliders. We calculate these effects with a plugin for adding ISR in MadGraph [25], and find that the cross sections are reduced by approximately 10%. For the sake of convenience, we use a uniform reduced ratio of 10% to estimate these effects when calculating signal significance.

We evaluate statistical significance (SS) using the Poisson formula [26] as follows:

$$SS = \sqrt{2L[(\sigma_S + \sigma_B)\ln(1 + \frac{\sigma_S}{\sigma_B}) - \sigma_S]}, \tag{8}$$

where L is the integrated luminosity of the collider, and σ_S, σ_B are the signal and background cross sections after our cuts, respectively.

The 2σ exclusion limit in $R - m_{T_+}$ plane at $\sqrt{s} = 2$, 3 TeV is shown in figure 4, where we also display the limit from the direct search at LHC-13 TeV [27], and the indirect limit based on a global fit of electroweak precision observables (EWPO) and Higgs data. A global fit of the EWPO and the latest Higgs data was conducted in our previous paper [28]; here, we consider the limit for case A, which is the default case in the literature. We note that the limit on the top partner mass ($m_{T_+} > 1300$ GeV) from the current direct search is consistent with indirect measurements, i.e., the global fit of the EWPO and the Higgs data. For $\sqrt{s} = 2$ TeV,

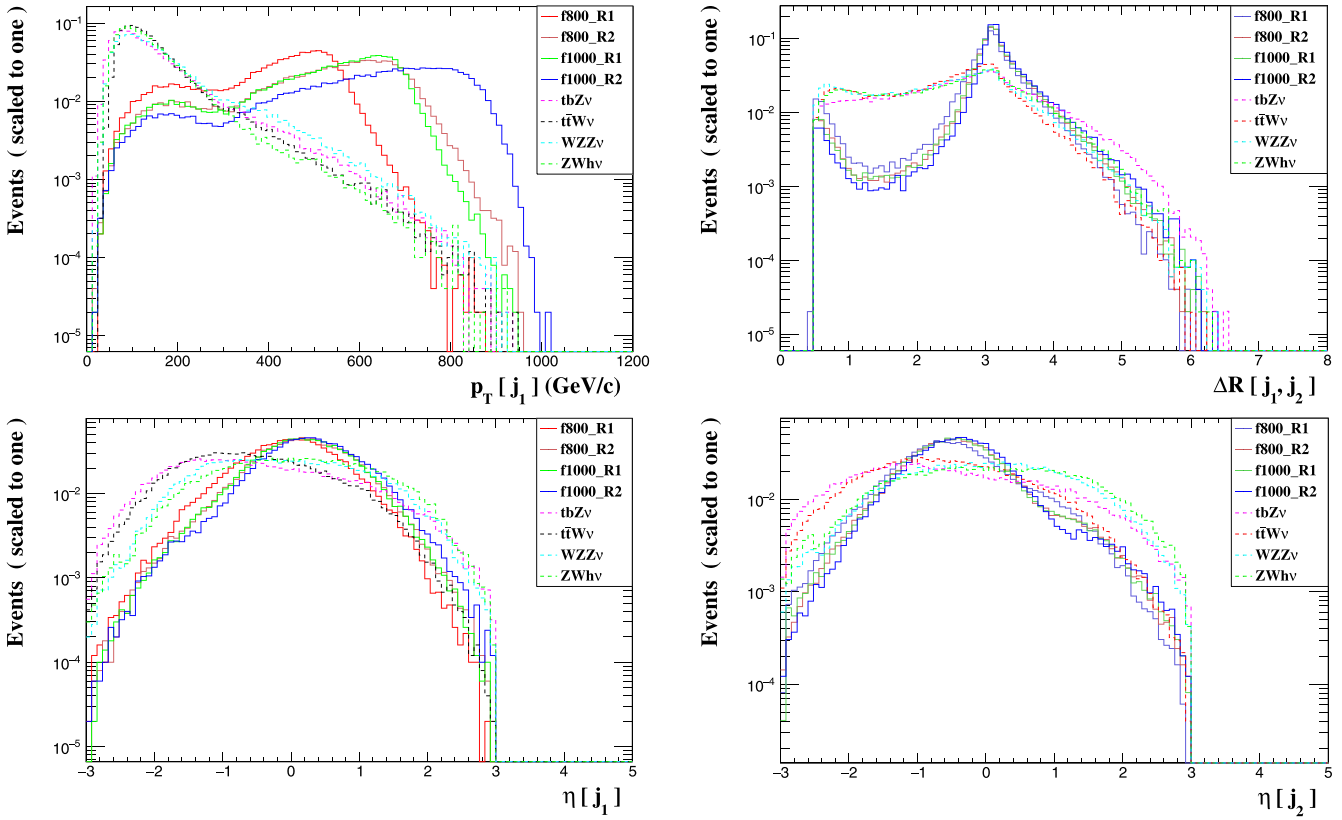

Figure 5. Normalized distributions of $p_T(j_1)$, $\Delta R(j_1, j_2)$, $\eta(j_1)$, $\eta(j_2)$ in the polarized signals and backgrounds for the four signal benchmark points at $\sqrt{s} = 2$ TeV in mode B.

we note that the excluding ability of $e\gamma$ collision is comparable to the LHC-13 TeV limit, if an integrated luminosity of 2000 fb^{-1} is achieved. For $\sqrt{s} = 3$ TeV, we note that the excluding ability of $e\gamma$ collision is noticeably enhanced, as compared with the case at $\sqrt{s} = 2$ TeV. The excluding ability of $e\gamma$ collision at $\sqrt{s} = 3$ TeV, with an integrated luminosity of 1000 fb^{-1}, is comparable to the LHC-13 TeV limit. If an integrated luminosity of 3000 fb^{-1} can be achieved, then top partner mass m_{T_+} can be excluded up to 1350 GeV. If we consider ISR effects, the limits on the top partner mass are reduced by approximately 10 GeV. In addition, we note that the excluding ability for the LHT parameter space at $e\gamma$ collision, and the current experimental limits, complement each other.

3.2. Mode B, $W^- \to l^- \bar{\nu}_l$ and $Z \to jj$

In this section, we will study the excluding ability of $e\gamma$ collision on top partner mass in mode B. As with mode A, the main difference between the signal and the backgrounds originates from the Z boson and its decay products. In addition, we find that there is no good distinction between the b-jet and lepton distributions of signals and backgrounds. We therefore select light jet cuts in order to improve the signal-to-background ratio. In regard to $\sqrt{s} = 2$ TeV, and $\sqrt{s} = 3$ TeV, these also exhibit similar kinematic distributions, and we therefore use the same cuts for them. In figure 5, we show the related normalized distributions of $p_T(j_1)$, $\Delta R(j_1, j_2)$, $\eta(j_1)$, and $\eta(j_2)$ as the polarized signals and backgrounds for the four signal benchmark points at $\sqrt{s} = 2$ TeV. We note that the leading order jet in signal events exhibits greater transverse momentum than in the backgrounds, due to the large mass of the top partner. The peak of $\Delta R(j_1, j_2)$ is at $\sim$3.14, which indicates that the two jets incline to fly back-to-back. Following analysis, we impose the following cuts to enhance signal significance:

$$\begin{aligned} &\text{Trigger: } N(j) \geqslant 2; \\ &\text{Cut} - 1\text{: } p_T(j_1) > 300\ \text{GeV}; \\ &\text{Cut} - 2\text{: } \Delta R(j_1, j_2) > 2.8; \\ &\text{Cut} - 3\text{: } -1.0 < \eta(j_1) < 1.0; \\ &\text{Cut} - 4\text{: } -1.4 < \eta(j_2) < 0.2. \end{aligned}$$

For clarity, we summarize the cut flows of the signals and backgrounds for the four signal benchmark points in table 3. After these cuts, we note that the backgrounds are suppressed, and the signals are effectively retained. For the four benchmarks, the cut efficiencies of the signal achieve 46%(34%), 55%(50%), 56%(47%), and 56%(57.8%) for $\sqrt{s} = 2$ TeV, and ($\sqrt{s} = 3$ TeV), respectively. In the following calculations, we use the same cuts for all signal parameter points at $\sqrt{s} = 2$, 3 TeV. Similarly to mode A, we apply a uniform reduced ratio of 10% in order to estimate ISR effects on calculations for signal significance.

The 2σ exclusion limit in $R - m_{T_+}$ plane at $\sqrt{s} = 2$, 3 TeV is shown in figure 6, where the limit from the direct search at LHC-13 TeV and the indirect limit from the global fit of EWPO and Higgs data are also displayed. We note that the excluding ability of $e\gamma$ collision in mode B is stronger than that in mode A. For $\sqrt{s} = 2$ TeV, the excluding ability

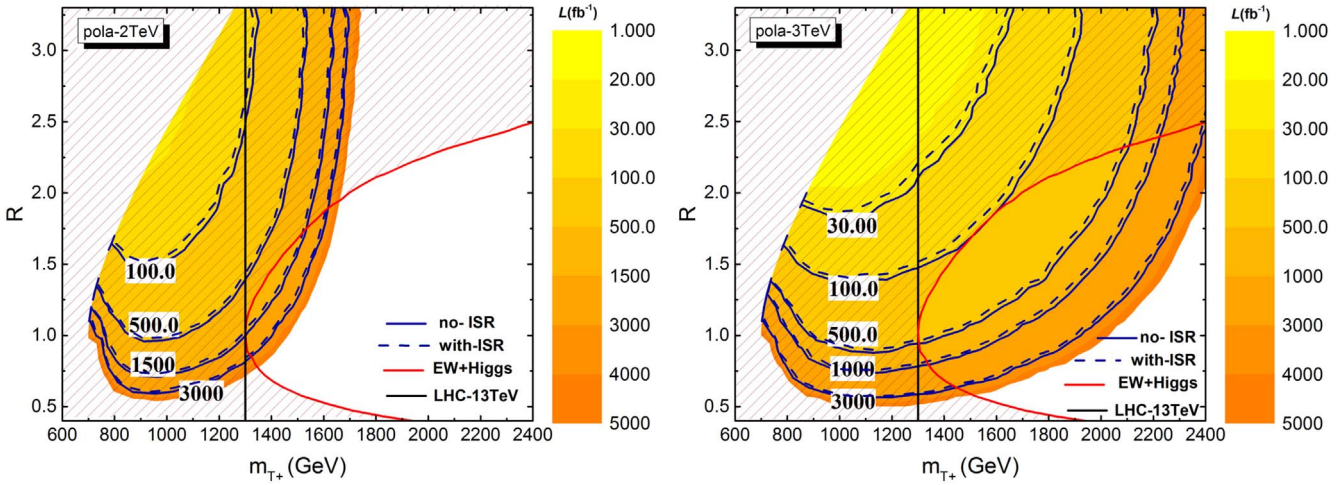

Figure 6. Data displayed as in figure 4, in relation to mode B.

Table 3. Cut flows of signal and backgrounds at $\sqrt{s} = 2.0$ TeV and $\sqrt{s} = 3.0$ TeV (in parentheses), with polarized beam, for the four signal benchmark points.

	Signals ($\times 10^{-3}$fb)				Backgrounds ($\times 10^{-3}$fb)			
Benchmarks	f800_R1	f800_R2	f1000_R1	f1000_R2	$tbZ\nu$	$t\bar{t}W\nu$	$WZZ\nu$	$ZWh\nu$
Original	55(93)	63(185)	20(52)	8.6(85)	501(787)	1315(2413)	1459(2873)	606(1213)
Trigger	54(91)	62(182)	20(51)	8.5(84)	487(757)	1314(2411)	1448(2844)	603(1204)
cut1	40(69)	52(157)	17(43)	7.5(76)	53(141)	119(343)	207(632)	43(141)
cut2	33(55)	47(138)	15(38)	7.0(70)	28(80)	63(183)	100(333)	23(84)
cut3	31(45)	43(120)	14(33)	6.1(61)	22(50)	48(106)	75(195)	19(56)
cut4	25(32)	35(93)	12(25)	4.9(49)	14(24)	33(51)	38(79)	11(23)
Total Eff.	46% (34%)	55% (50%)	56% (47%)	56% (57.8%)	2.7% (3%)	2.5% (2.1%)	2.6% (1.9%)	1.8% (1.9%)

of $e\gamma$ collision with an integrated luminosity of 1500 fb^{-1} is comparable to the LHC-13 TeV limit. For $\sqrt{s} = 3$ TeV, the excluding ability of $e\gamma$ collision with an integrated luminosity of 500 fb^{-1} is comparable to the LHC-13 TeV limit. If an integrated luminosity of 3000 fb^{-1} is achieved, the top partner mass m_{T_+} can be excluded up to 1440 GeV. Similarly, ISR effects will reduce the limits on the top partner mass by approximately 10 GeV. In addition, the signals in mode B have bigger cross sections, meaning that they can be detected more easily than those in mode A.

4. Conclusions

Based on the LHT model, we investigated the single production of the T-even top partner at the $e\gamma$ collider through channels $e^-\gamma \to \bar{T}_+ b\nu_e \to (\bar{t}Z)b\nu_e \to (W^-\bar{b}l^+l^-)b\nu_e \to (jj\bar{b}l^+l^-)b\nu_e$ (mode A) and $e^-\gamma \to \bar{T}_+ b\nu_e \to (\bar{t}Z)b\nu_e \to (W^-\bar{b}jj)b\nu_e \to (l^-\bar{\nu}_l\bar{b}jj)b\nu_e$ (mode B). We selected polarization degrees $P_{e^-} = -0.8$, and $P_\gamma = +1$, and center-mass energy values $\sqrt{s} = 2$ TeV, and $\sqrt{s} = 3$ TeV. We performed a fast detector simulation and selected kinematic cuts in order to improve statistical significance. For $\sqrt{s} = 2$ TeV, the excluding ability of the two modes do not exhibit great improvement compared with the current experimental limits. For $\sqrt{s} = 3$ TeV, however, the excluding ability of the two modes improved significantly. This is comparable to the current LHC-13 TeV limit with an integrated luminosity $L = 1000$ (500) fb^{-1} for mode A (B). If the integrated luminosity achieves 3000 fb^{-1}, then top partner mass $m_{T_+} \leqslant$ 1350 (1440) GeV can be excluded at 2σ level for mode A (B). For both modes, we also considered ISR effects, and found that the excluding ability of $e\gamma$ collision on the the top partner mass would be reduced by approximately 10 GeV. Moreover, the excluding ability for the LHT parameter space at $e\gamma$ collision complements the current experimental limits.

Acknowledgments

This work is supported by the National Natural Science Foundation of China (NNSFC) under grant No. 11405047.

References

[1] CMS Collaboration 2012 *Phys. Lett.* B **716** 30
[2] ATLAS Collaboration 2012 *Phys. Lett.* B **716** 1
[3] Susskind L 1979 *Phys. Rev.* D **20** 2619
[4] Randall L and Sundrum R 1999 *Phys. Rev. Lett.* **83** 3370
[5] Kaplan D B, Georgi H and Dimopoulos S 1984 *Phys. Lett.* B **136** 187
Vignaroli N 2012 *JHEP* **1207** 158

[6] Schmaltz M and Tucker-Smith D 2005 *Ann. Rev. Nucl. Part. Sci.* **55** 229
[7] Chacko Z, Goh H-S and Harnik R 2006 *JHEP* **0601** 108
[8] Martin S P 2010 *Phys. Rev.* D **81** 035004
[9] see recent examples, Dawson S and Furlan E 2014 *Phys. Rev.* D **89** 015012
Han C C, Kobakhidze A, Liu N, Wu L and Yang B F 2015 *Nucl. Phys.* B **890** 388–99
Basso1 L and Andrea J 2015 *JHEP* **02** 032
Reuter J and Tonini M 2015 *JHEP* **01** 088
Berger J, Hubisz J and Perelstein M 2012 *JHEP* **1207** 016
Liu N, Wu L, Yang B F and Zhang M C 2016 *Phys. Lett.* B **753** 664–9
Yang B F, Hou B F, Zhang H Y and Liu N 2019 *Phys. Rev.* D **99** 095002
Shang L L, Zhang D and Yang B F 2019 *Phys. Rev.* D **100** 075032
[10] ATLAS Collaboration 2017 *JHEP* **10** 141
ATLAS Collaboration 2017 *JHEP* **08** 052
ATLAS Collaboration 2019 *JHEP* **05** 164
[11] CMS Collaboration 2018 *Phys. Lett.* B **779** 82
CMS Collaboration 2018 *Phys. Lett.* B **781** 574
CMS Collaboration 2018 *JHEP* **08** 177
[12] CEPC Study Group arXiv:1809.00285
CEPC Study Group arXiv:1811.10545
[13] Barklow T, Brau J, Fujii K, Gao J, List J, Walker N and Yokoya K arXiv:1506.07830
Fujii K *et al* arXiv:1710.07621
[14] CLIC Conceptual Design Report (http://project-clic-cdr.web.cern.ch/project-clic-cdr/)
[15] Cheng H-C and Low I 2003 *JHEP* **0309** 051
Cheng H-C and Low I 2004 *JHEP* **0408** 061
Low I 2004 *JHEP* **0410** 067
[16] Particle Data Group 2018 *Phys. Rev.* D **98** 030001
[17] Alwall J *et al* 2014 *JHEP* **07** 079
[18] Sjostrand T, Mrenna S and Skands P Z 2006 *JHEP* **0605** 026
[19] de Favereau J *et al* 2014 *JHEP* **1402** 057
[20] Cacciari M, Salam G P and Soyez G 2012 *Eur. Phys. J.* C **72** 1896
[21] Cacciari M, Salam G P and Soyez G 2008 *JHEP* **04** 063
[22] Conte E, Fuks B and Serret G 2013 *Comput. Phys. Commum* **184** 222
Conte E, Dumont B, Fuks B and Wymant C 2014 *Eur. Phys. J.* C **74** 3103
[23] Shang L and Zhang Y EasyScan_HEP (https://easyscanhep.hepforge.org)
[24] Kuraev E A and Fadin V S 1985 *Sov. J. Nucl. Phys* **41** 466
Skrzypek M and Jadach S 1991 *Z. Phys.* C **49** 577
Chen P 1992 *Phys. Rev.* D **46** 1186
[25] A plugin for adding ISR in MadGraph (https://answers.launchpad.net/mg5amcnlo/+question/675354)
[26] Cowan G, Cranmer K, Gross E and Vitells O 2011 *Eur. Phys. J.* C **71** 1554
[27] Dercks D, Moortgat-Pick G, Reuter J and Shim S Y 2018 *JHEP* **05** 049
[28] Yang B F, Mi G F and Liu N 2014 *JHEP* **10** 047
Yang B F, Han J Z and Liu N 2017 *Phys. Rev.* D **95** 035010
Yang B F, Zhang H Y, Hou B F and Liu N 2018 *Chin. Phys.* C **42** 103102